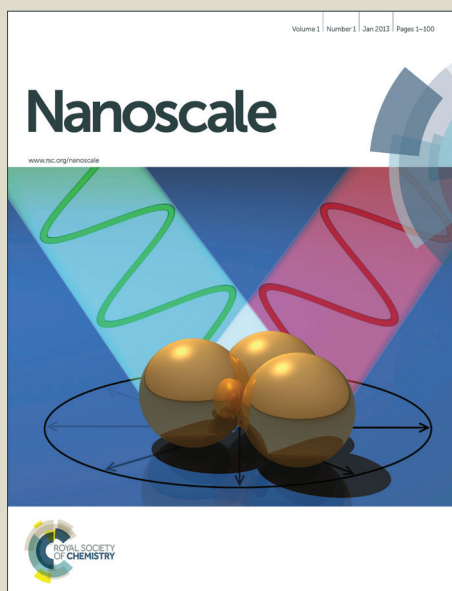


Nanoscale

Accepted Manuscript



This is an *Accepted Manuscript*, which has been through the Royal Society of Chemistry peer review process and has been accepted for publication.

Accepted Manuscripts are published online shortly after acceptance, before technical editing, formatting and proof reading. Using this free service, authors can make their results available to the community, in citable form, before we publish the edited article. We will replace this *Accepted Manuscript* with the edited and formatted *Advance Article* as soon as it is available.

You can find more information about *Accepted Manuscripts* in the [Information for Authors](#).

Please note that technical editing may introduce minor changes to the text and/or graphics, which may alter content. The journal's standard [Terms & Conditions](#) and the [Ethical guidelines](#) still apply. In no event shall the Royal Society of Chemistry be held responsible for any errors or omissions in this *Accepted Manuscript* or any consequences arising from the use of any information it contains.



Anisotropic thermal transport in phosphorene: Effects of crystal orientation

Te-Huan Liu,^a and Chien-Cheng Chang^{*ab}

Received 00th January 20xx,
Accepted 00th January 20xx

DOI: 10.1039/x0xx00000x

www.rsc.org/

As an intrinsic thermally anisotropic material, the thermal properties of phosphorene must be varying with respect to the crystal chirality. Nevertheless, previous studies of the heat transfer in phosphorene are limited to the 0.0° (zigzag, ZZ) and 90.0° (armchair, AC) chiralities. In this paper, we investigate the orientation-dependent thermal transport in phosphorene sheets with a complete set of crystal chirality ranging from 0.0° to 90.0° by using the Boltzmann transport equation (BTE) associated with the first-principles calculations. It is found that in the phosphorene sheets, the intrinsic thermal conductivity is a smooth, monotonic decreasing function of the crystal chirality, which exhibits a sinusoidal behavior bounded by the two terminated values 48.9 (0.0°) and 27.8 (90.0°) W/mK. The optical modes have unusually large contributions to heat transfer, which account for almost 30 % of the total thermal conductivity of phosphorene sheets. This is due to the fact that the optical phonons have comparable group velocities and relaxation times with the acoustic phonons.

1 Introduction

According to the existing library of two-dimensional (2D) crystals, the 2D materials can be classified into three subcategories: the graphene family, 2D chalcogenides and 2D oxides.¹ Nevertheless, phosphorene, a new type of 2D material consisting of sp^3 -hybridized phosphorus atoms with puckered structure, has been successfully exfoliated from black phosphorus in 2014,^{2,3} and presently catch the scientific community's eye not only because of its novelty, but also the unusual physical properties.²⁻¹⁰ As the first discovered 2D material, graphene is largely limited for use in electronic nanodevices due to the absence of a bandgap. Several strategies have been proposed to open the gap which, however, is always accompanied with the massive losses of electronic mobility.¹¹⁻¹³ Unlike graphene, phosphorene manifests a direct as well as tunable transport gap from 0.3 (30 layers) to 1.0 (monolayer) eV.¹⁴ On the other hand, although the transition-metal chalcogenides (TMDs) such as molybdenum disulfide (MoS_2) and Tungsten diselenide (WSe_2) have a moderate bandgap, their carrier mobilities are much lower than that of phosphorene which is found to be $\sim 1000 \text{ cm}^2/\text{Vs}$.² From these observations, phosphorene is arguably an appealing contender of next-generation nanodevices by means of its extraordinary

properties. In fact, many recent studies have demonstrated that phosphorene can be implemented in field-effect transistors with very high on-off ratio around 10^4 to 10^5 ,^{1,2,14} in wide-range photodetectors operating from visible to near-infrared regime,¹⁵ and in high-performance Lithium-Ion battery.¹⁶

Another important issue of phosphorene is the thermal transport in thermoelectric devices. The thermoelectric efficiency can be quantitatively described in terms of the figure of merit, $ZT = TS^2\sigma/\kappa$, where T , S , σ and κ respectively refer to the temperature, thermopower, electronic conductivity and thermal conductivity.¹⁷ As we know, a poor thermal conductor is needed because it can maintain the temperature gradient and thus impart a higher thermoelectric efficiency than that of a good conductor. The reported ZT value of phosphorene nanoribbon can be as high as 6.4 at room temperature from first-principles calculations.¹⁸ Very recently, Liao *et al.*¹⁹ report a lower electron mobility ($\sim 170 \text{ cm}^2/\text{Vs}$ at 300 K) and ZT value (0.31 at 500 K) through the ab initio calculations. This notable study reveals that previous calculations might overestimate the carrier mobility due using deformation potential.

To the best of the authors' knowledge, measured data of thermal conductivity of phosphorene have not been presented so far, yet, some calculations of thermal properties have been done. The thermal conductivities of phosphorene calculated by Fei *et al.*²⁰ are around 50.0 and 20.0 W/mK in ZZ and AC directions, respectively; they also obtained the figure of merit $ZT = 1.0$ of phosphorene with the doping density $2 \times 10^{16} \text{ m}^{-2}$ at 300 K. The calculations done by Qin *et al.*²¹ show lower values, which are 30.2 and 13.7 W/mK along the corresponding transport directions. It is noted as a remark that Ong *et al.*²² calculated the thermal conductance in the ZZ and AC directions of phosphorene from 0 to 1000 K. They found that the thermal

^a Institute of Applied Mechanics, National Taiwan University, 1 Sec. 4, Roosevelt Road, Taipei 106, Taiwan. E-mail: mechang@iam.ntu.edu.tw

^b College of Mechanical Engineering, Guangxi University, 100 Daxue Road, Nanning 530004, China. E-mail: mechang@gxu.edu.cn

† Footnotes relating to the title and/or authors should appear here. Electronic Supplementary Information (ESI) available: [details of any supplementary information available should be included here]. See DOI: 10.1039/x0xx00000x

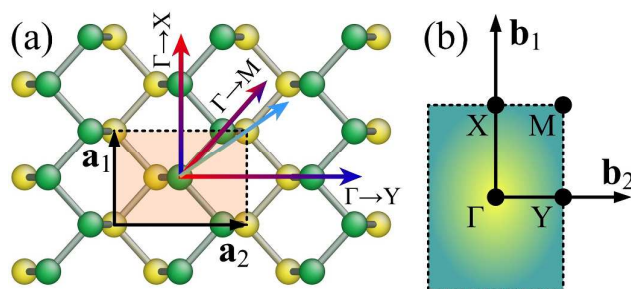


Fig. 1 (a) Primitive unit cell and (b) first Brillouin zone of phosphorene. The three high-symmetry directions Γ -X (0.0°), Γ -M (35.5°) and Γ -Y (90.0°) are indicated by arrows in real lattice. The light-blue arrow indicates the 54.5° transport direction. The atoms colored by green and yellow are used to distinguish the atoms' location of height—they are all phosphorus atoms.

conductance in the ZZ and AC directions will saturate to different constant values at high temperatures, and increasing the external strains will give rise to increase in the thermal conductance anisotropy. Zhu *et al.*²³ investigated the thermal conductivity of phosphorene with respect to different grain sizes; the thermal conductivity in the ZZ direction is size-dependent varying from 75.0 to 83.5 W/mK, whereas in the AC direction is size-independent and takes the value 24.3 W/mK. These theoretical works have revealed that the phosphorene possesses a low thermal conductivity at room temperature, and most importantly, it would be thermally anisotropic.

From the symmetry analysis for crystals, we know that the system's thermal conductivity will be isotropic when the order of symmetry is higher than C_3 rotation.^{24,25} For instance, the hexagonal lattice system with C_6 symmetry such as graphene,^{26,27} MoS₂²⁸ and even blue phosphorene²⁹ are thermally isotropic; the anisotropy emerges when the phonon confinement effects and boundary scatterings become dominant, *i.e.* the thermal transport in nanoribbons. In contrast, the primitive cell as well as the first Brillouin zone (FBZ) of phosphorene are orthorhombic as shown in Figs. 1(a) and 1(b), respectively, hence the C_2 symmetry will naturally introduce anisotropy in heat conduction. However, previous studies of thermal transport in phosphorene are focused on the ZZ and AC directions.^{10,20-23,25,29} Yet, the heat transport in other crystal directions which is crucially important in an intrinsic anisotropic material remains unexplored. In this paper, we calculate the thermal properties of phosphorene by using the Boltzmann transport equation under relaxation time approximations associated with the first-principles calculations. The primary goal is to explore the thermal conductivity in a complete set of crystal chirality (*i.e.* transport direction) ranging from $\theta=0.0^\circ$ (ZZ) to 90.0° (AC), which benefits one to find out the optimized transport directions in practical applications.

2 Methodology

2.1 BTE analysis

In order to investigate the thermal transport properties of phosphorene, we start with the BTE under the relaxation time approximation³⁰

$$\frac{\partial f}{\partial t} + \mathbf{v} \cdot \nabla f = -\frac{f - f_0}{\tau_{eff}} \quad (1)$$

where f is the statistical distribution function of an ensemble of phonons, and f_0 is the distribution function at the equilibrium state, \mathbf{v} and τ_{eff} represent the phonon group velocity and effective phonon relaxation time, respectively. In the steady state, by definition $\partial f / \partial t = 0$, the distribution function can be written to first order expansion as $f = f_0 - \tau_{eff} \frac{df_0}{dT} \mathbf{v} \cdot \nabla T$. For a material with volume V , one can calculate the heat flux by summing over the possible wavevectors \mathbf{k} in the first Brillouin zone and over the polarization modes s , $\mathbf{J} = \frac{1}{V} \sum_s \sum_{\mathbf{k}} \varepsilon_{\mathbf{k}} \mathbf{v}_{\mathbf{k}} f$; here $\varepsilon = \hbar\omega$ is the phonon energy. In the real space, the phonons, carrying different frequencies, propagate in all directions through the entire crystal. By considering the 2D solid angle, we have $\mathbf{J} = \sum_s \int_0^{\omega_{max}} \int_0^{2\pi} \varepsilon \mathbf{v} f \frac{D}{2\pi} d\theta d\omega$, where D is the normalized phonon density of state (PDOS) per unit volume, and $f_0 = [\exp(\hbar\omega/k_B T) - 1]^{-1}$ is the Bose-Einstein distribution. It is worthy of a note that the integral of $\mathbf{v} f_0$ vanishes because it is an odd function, which is in conformity with the fact that the net heat flux is zero at the equilibrium state. Now we cast the heat flux into the form of Fourier's law for heat conduction, $\mathbf{J} = -\kappa \nabla T$, thereby obtaining the general expression of thermal conductivity in the i crystal chirality (i transport direction):³⁰

$$\kappa_i = \frac{k_B}{2\pi} \sum_s \int_0^{\omega_{max,i}} \int_0^{2\pi} v_i^2 D_i \tau_{eff,i} \frac{\xi_i^2 e^{\xi_i}}{(e^{\xi_i} - 1)^2} d\theta d\omega \quad (2)$$

where $\xi_i = \hbar\omega_i/k_B T$ is a non-dimensional parameter. Here the phonon group velocity is a function of the frequency. The component of the velocity in the i chirality is given by $v_i = |\nabla_{\mathbf{k}} \omega_i| \cos \theta_r$, where θ_r is the relative angle of the individual phonon's motion direction from the thermal transport direction under concern (main transport direction). Therefore, the full-band phonon dispersion relations should be taken into account. In 2D solid, the phonons are excited and travel in arbitrary directions along the basal plane; each individual phonon will contribute a part of thermal conductivity in the i crystal chirality depending on the projection of its incident direction on the main transport direction. All of their contributions should be considered and integrated through Eq. (2) to obtain the κ_i .

In this study, the phonon-boundary and phonon-phonon (umklapp) scattering should be taken into account to calculate the intrinsic thermal conductivity. We use the empirical expressions to describe the two mechanisms in the BTE analysis. The phonon-boundary interaction can be described in a totally diffusive form,³¹

$$\tau_{B,i}^{-1} = \frac{2|\nabla_{\mathbf{k}} \omega_i| \cos \theta_r}{l} \quad (3)$$

where l represents the length of the sheet. The phonon group velocity is projected on the directions to the main transport direction. Thus, the boundary scattering rate (inverse of scattering time) can be obtained from the parallel component of

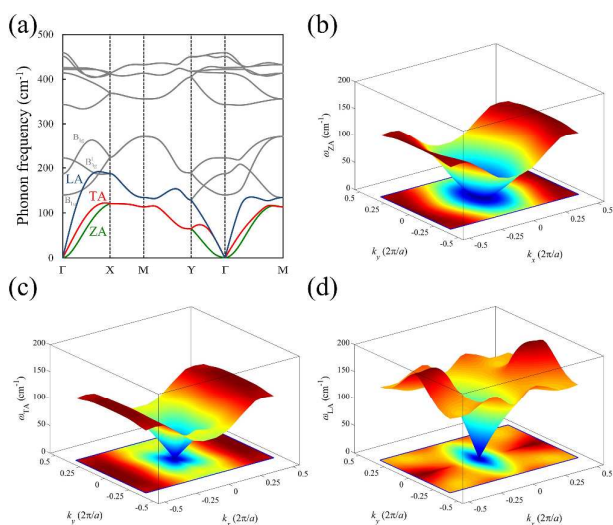


Fig. 2 Full-band phonon dispersion relations of phosphorene. (a) Along the high-symmetry directions. The surface and contour of (b) ZA mode, (c) TA mode, and (d) LA mode.

phonon group velocity divided by the phonon's travelling distance. The phonon-phonon scattering is given by³²

$$\tau_{U,i}^{-1} = \frac{\hbar \gamma_i^2 \omega_i^2}{m \Theta_i |\nabla_{\mathbf{k}} \omega_i|^2} T e^{-\Theta_i/3T} \quad (4)$$

where m and γ_i are, respectively, the mass of basis atom and the Grüneisen parameter. The Debye temperature Θ_i of the i crystal chirality is calculated by $\Theta_i^2 = (5\hbar^2/3k_B^2) \int_0^{\omega_{max,i}} \omega_i^2 D_i d\omega$. The umklapp scattering starts to dominate when the temperature increases beyond the Debye temperature, which is due to the enhancement of the anharmonicity of lattice vibrations. This is the reason why Glassbrenner *et al.* treat the scattering rate such that it is proportional to $\gamma_i^2 T/\Theta_i$ in their original paper.³² This semi-empirical formula has been well used to calculate the thermal conductivity of group IV and III-V semiconductors.³³ Finally, we can obtain the effective phonon relaxation time by using the Matthiessen's rule, $\tau_{eff,i}^{-1} = \tau_{B,i}^{-1} + \tau_{U,i}^{-1}$.

2.2 Details of first-principles calculations

The first-principles calculations are carried out by using Quantum ESPRESSO package,³⁴ and the ultrasoft pseudopotential with Perdew-Burke-Ernzerhof (PBE) exchange-correlation functional is employed to describe the interactions between phosphorus atoms. The cutoff energy of the wave function and the energy convergence threshold are set as 550 and 10^{-11} eV, respectively. The structure optimization is done for the unit cell with the $24 \times 32 \times 1$ Monkhorst-Pack k -grid until the Hellmann-Feynman forces acting on the basis atoms are smaller than 10^{-5} eV/Å. The optimized lattice constants are 3.31 (ZZ) and 4.62 Å (AC), which are in good agreement with those found in previous studies.³ The $8 \times 8 \times 1$ q -grid is used in the follow-on phonon dispersion calculations. The convergence threshold for self-consistent calculations of the dynamical matrix should be less than 10^{-20} eV to avoid the negative frequencies appearing in the proximity of zone center.

3 Results and discussions

3.1 Phonon dispersions and Grüneisen parameters

The phonon dispersion curves of phosphorene along the high-symmetry directions are plotted in Fig. 2(a). The directions labeled as Γ -X, Γ -M and Γ -Y in the reciprocal space are corresponding to the crystal chiralities $\theta=0.0^\circ$ (ZZ), 35.5° and 90.0° (AC) in the real space, respectively. On the other hand, the diagonal transport direction of the unit cell indicated by the light-blue arrow in Fig. 1(a) is also of interest, which has the chirality $\theta=54.5^\circ$, a complementary angle with the Γ -M direction. Figs. 2(b) to 2(d) demonstrate the full-band surfaces and contours of the three acoustic phonon modes. We can find that the phonon group velocities manifest significant anisotropy within the entire FBZ, which are much different from those of graphene and hexagonal boron nitride (h-BN).^{35,36} For the ZA and LA modes, the 0.0° chirality owns the highest group velocity, 0.56 and 8.64 km/s, respectively, but the values monotonically decrease to 0.50 and 4.07 km/s when the chirality increases to 90.0° . In contrast, the phonon group velocity of TA mode is not monotonically decreasing with respect to the lattice orientation, yet a minimum value occurs at the 54.5° chirality; the group velocities along 0.0° , 54.5° and 90.0° are 4.00, 3.48 and 4.20 km/s, respectively. Fig. 2(a) shows the Grüneisen parameters of phosphorene along the high-symmetry directions. Apparently, the Grüneisen parameters are also anisotropic because they are calculated by means of the phonon dispersion relation, $\gamma_i = -(V/\omega_i) \partial \omega_i / \partial V$. It is interesting that the Grüneisen parameter in phosphorene is orientation-dependent at Γ point, and the discontinuities existing in these acoustic branches can be easily observed. This fact indicates that the anharmonicity near the zone center is much different from one phonon wavevector to another. As a

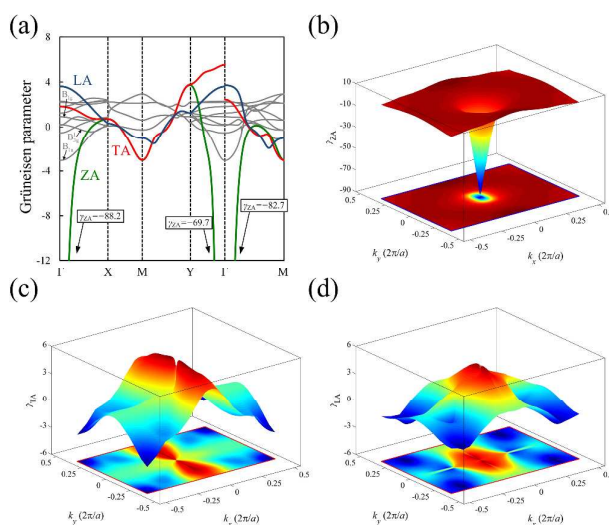


Fig. 3 Full-band Grüneisen parameters of phosphorene. (a) Along the high-symmetry directions. The surface and contour of (b) ZA mode, (c) TA mode, and (d) LA mode. The Grüneisen parameters are calculated by changing the lattice with $\pm 0.25\%$ of biaxial strains.

semiconductor, the phosphorene has its thermal conductivity majorly contributed from the lattice vibrations, in particular, the long-wavelength phonons due to their higher group velocity and weaker scattering. Therefore, we can attribute the intrinsic anisotropy in phosphorene to the orientation-dependent phonon group velocity and Grüneisen parameter.

3.2 Thermal conductivity with different chiralities

Fig. 4 shows the thermal conductivities of 1.0 μm -length phosphorene sheets with different crystal chiralities ranging from 0.0° to 90.0° at 300 K. The thermal conductivities along the 0.0° and 90° chiralities are 48.9 and 27.8 W/mK, respectively, which are in good agreement with Fei *et al.*'s results,²⁰ and have the same order of magnitude with other previous studies.^{10,20-23,25,29} We further find that the thermal conductivity manifests a smooth, monotonic decreasing trend with increasing the crystal chirality. It is natural to fit the results by a cosine function with period 2π , $\kappa(\theta)=10.53\times\cos(2\theta)+38.42$, as plotted in Fig. 4. This cosine function captures well the crystal symmetry from 0° to 180° with a small error standard deviation 0.68 %. This result may offer us a route to roughly predict the trend of thermal conductivity with respect to the crystal chirality in such C_2 -symmetry materials. On the other hand, we could define the anisotropy rate by $AR(\theta)=\{[\kappa(0^\circ)-\kappa(\theta)]/\kappa(0^\circ)\}\times 100\%$, which takes the values 15.1, 29.8 and 43.0 % in the 35.5° , 54.5° and 90.0° chiralities, respectively. The anisotropy rate can also be fitted by a cosine function $AR(\theta)=21.51\times[1-\cos(2\theta)]$. The calculated result of phosphorene sheet in the 90.0° chirality shows an astonishing anisotropy rate, which is almost four times larger than that obtained for the AC graphene nanoribbons ($\sim 12.3\%$) from very similar analysis.³⁵

Fig. 5(a) shows the temperature-dependent thermal conductivity along the 0.0° , 35.5° , 54.5° and 90.0° chiralities,

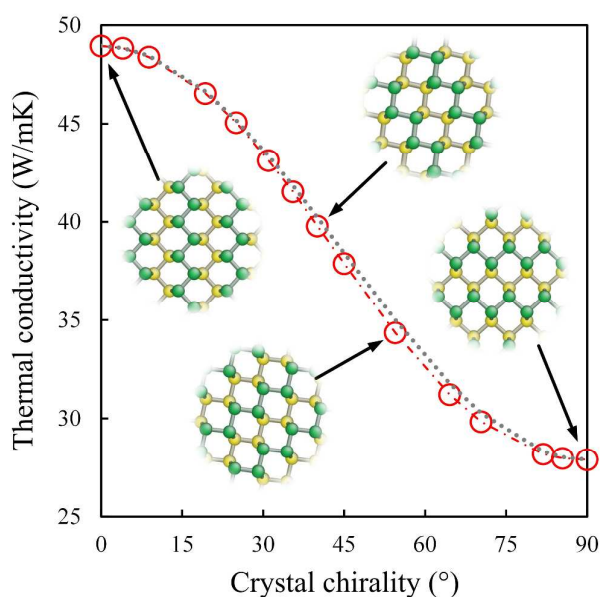


Fig. 4 Orientation-dependent thermal conductivity of 1.0 μm -length phosphorene sheet. The gray dot line is fitted by cosine function with period 2π .

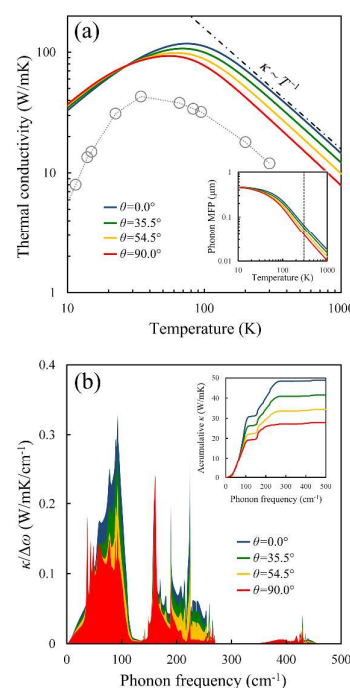


Fig. 5 (a) Temperature-dependent thermal conductivity of phosphorene sheets. The blue, green, yellow and red lines represent the thermal conductivity along 0.0° , 35.5° , 54.5° and 90.0° chiralities, respectively. The gray circles are the data of bulk black phosphorus from experimental measurement.³⁷ The inset shows the phonon MFP as a function of temperature. (b) The distribution function of thermal conductivity of phosphorene sheets at 300 K. The thermal conductivity can be computed by the area under distribution function, and the corresponding accumulated functions of thermal conductivity of these chiralities are shown in the inset.

in which the lines represent the 1.0 μm -length phosphorene sheet. The calculated thermal conductivities of phosphorene sheets are larger than that of bulk black phosphorus measuring from experiment.³⁷ The phosphorene nanoribbons show the ultrahigh AR when the dimension ratio l/w is large, provided that we do not consider edge reconstruction. Furthermore, at high temperatures, we can find that the thermal conductivities are in exactly T^{-1} dependence for phosphorene sheets while the temperature respectively exceeds the characteristic 200 K due to the presence of the umklapp scattering. It is also interesting that the 90.0° chirality has the highest thermal conductivity at the very low temperatures, yet has the lowest value with the raising the temperature because of its smaller phonon group velocities and larger Grüneisen parameters. The thermal transport is limited by the boundary scatterings at low temperature, where the relaxation time is inversely proportional to the phonon group velocities (Eq. (3)). On the other hand, the umklapp scattering is dominant in high temperature region, where the relaxation time decreases with increasing the square of the ratio $\gamma_i/|\mathbf{V}\mathbf{k}\omega_i|$ (Eq. (5)).

Qin *et al.*²¹ and Jain *et al.*²⁹ have demonstrated that the phonons with MFP between 10 nm to 1.0 μm are responsible for the 90 % thermal conductivity in phosphorene. In view of this, we further compute the effective phonon MFP $\lambda_{eff,i}$ of phosphorene as shown in the inset of Fig. 5(a), which is given by

$$\lambda_{eff,i} = \frac{\sum_s \int_0^{\omega_{max,i}} \int_0^{2\pi} v_i^2 D_i \tau_{eff,i} \frac{\xi_i^2 e^{\xi_i}}{(e^{\xi_i} - 1)^2} d\theta d\omega}{\sum_s \int_0^{\omega_{max,i}} \int_0^{2\pi} v_i D_i \frac{\xi_i^2 e^{\xi_i}}{(e^{\xi_i} - 1)^2} d\theta d\omega} \quad (5)$$

This expression has been employed to extract the phonon MFP of graphene and MoS₂ in our previous studies.^{28,38} The obtained values for the 0°, 35.5°, 54.5° and 90.0°-chirality phosphorene sheets at 300 K are 65.4, 56.5, 47.5 and 39.5 nm, respectively, which is much less than graphene (~750.0 nm),³⁹ but larger than MoS₂ sheet (around tens nm).^{28,40,41} The calculations indicate that the phonon MFP decreases with increasing the chirality, and can be described by a cosine function, $\lambda_{eff}(\theta) = 12.95 \times \cos(2\theta) + 52.45$. In addition, we calculate the distribution function of the thermal conductivity with respect to the phonon frequency of phosphorene sheets as plotted in Figs. 5(b). The distributions show significant redshift as the chirality increases, and as a consequence, the thermal conductivity in phosphorene decreases. On the other hand, the thermal conductivity is majorly contributed by the frequencies in the range between 0 and 270 cm⁻¹, which means that the optical modes under the phonon bandgap also have non-negligible contributions. Based on the discussions above, we recognize that the acoustic modes are not the only effective channels in heat conduction in phosphorene, and it is of significant importance to examine the behaviors of optical modes.

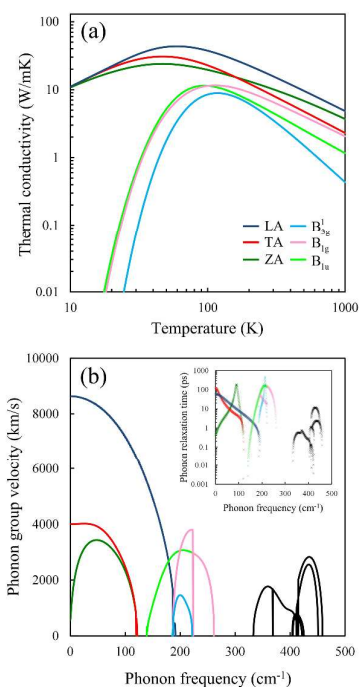


Fig. 6 (a) Temperature-dependent thermal conductivity of 0.0°-chirality phosphorene sheet with different phonon modes. (b) The phonon group velocity of phosphorene sheet along 0.0° chirality with different phonon modes; the corresponding phonon relaxation times are plotted in the inset. The black lines and labels represent the other six optical modes over the phonon bandgap.

3.3 Optical modes in phosphorene

Fig. 6(a) shows the mode thermal conductivity in the 0.0° chirality of the 1.0 μm-length phosphorene sheet. The vibration patterns of these modes have been studied in great details in Cai *et al.*'s work.¹⁰ The ZA, TA, LA and rest optical modes respectively, account for 20.7, 16.6, 32.0 and 30.7 % of the total thermal conductivity in the phosphorene sheets at room temperatures. This finding indicates that the three optical modes under the phonon bandgap—B_{1u}, B_{1g} and B_{3g} modes—have substantial contributions to the thermal transport. Finally, it is worthwhile to give an explanation to the optical phonons, which possess such high proportion in the thermal conductivity. Fig 6(b) shows that the group velocities of B_{1u}, B_{1g} and B_{3g} modes are similar to the ZA and TA modes; in addition, the relaxation times of these optical phonons are in the same order of magnitude with the acoustic phonons as displayed in the inset of Fig. 6(b). These facts feature the optical phonons having MFPs comparable to the acoustic phonons, and that is the reason why they cannot be ignored in the heat transfer in phosphorene.

3.4 Anisotropic rate in nanoscale

In the practical design of nanodevices, the amount of anisotropy on the nanoscale is of more interest. In order to characterize the finite-width effect, we need to include the phonon-edge scattering³¹

$$\tau_{E,i}^{-1} = \frac{|\nabla_{\mathbf{k}} \omega_i| \sin \theta_r}{w} \left(\frac{1 - p_i}{1 + p_i} \right) \quad (6)$$

where w represents the width of the sheet. The edge specularity is calculated by $p_i = \exp(-4|\mathbf{k}_i|^2 \Delta^2 \sin^2 \theta_r)$, and Δ is the root-mean-square (rms) edge roughness: the larger roughness, the smaller specularity. The edge reconstruction is of crucial importance in the calculation of edge roughness, particularly in 2D materials,^{42,43} which will largely influence the estimation of the phonon-edge scattering. Our model employs the minimum rms edge roughness of each nanoribbon (0.74 Å for ZZ and 0.83 Å for AC edge), and thus cannot take into account the edge

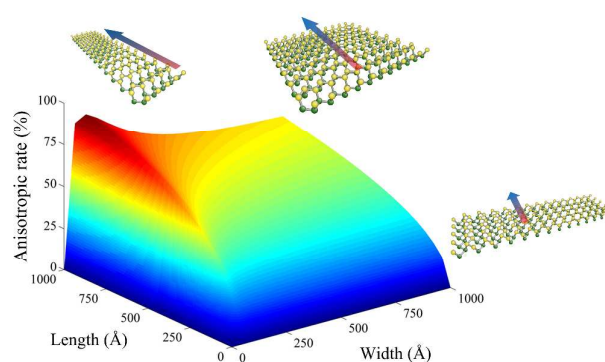


Fig. 7 The surface of AR between the ZZ and AC directions of the phosphorene with the size of sheet up to 1000 Å×1000 Å. The dimensional resolution is 50 Å×50 Å, and the direction of thermal transport is parallel to the dimension l .

reconstruction. Hence, we have to emphasize that the following results are only valid when the nanoribbons are cut perfectly and the edge reconstruction is absent. The calculated AR between the ZZ and AC directions of phosphorene nanoribbons with different dimensions ($l \times w$) of sheet as plotted in Fig. 7. The result clearly demonstrates that the AR increases with increasing the dimension ratio l/w —an ultrahigh $AR=86.4\%$ is observed in the phosphorene nanoribbon with sheet size $1000 \text{ \AA} \times 50 \text{ \AA}$, whereas a relative low $AR=16.3\%$ happens in the sheet $50 \text{ \AA} \times 1000 \text{ \AA}$. This can be explained by the difference in the edge roughness of the 0° and 90° chiralities, which will further enhance the thermal anisotropy between the two transport directions when the width of the phosphorene nanoribbon is on the nanoscale.

4 Conclusions

In this study, we investigate the orientation-dependent thermal transport of phosphorene by using the BTE analysis associated with the first-principles calculations. The main findings include: (1) the phosphorene is an intrinsic thermally anisotropic material. The thermal conductivity of the phosphorene sheet manifests a smooth, monotonic decreasing behavior with increasing the crystal chirality from 0.0° (ZZ) to 90.0° (AC), which can be well fitted by a cosine function in the complete set of chirality. (2) We demonstrate that the optical modes are responsible for the unusual high thermal conductivity in phosphorene sheets. This can be attributed to the fact that the B_{1u} , B_{1g} and B_{3g}^1 modes have comparable phonon MFPs with the acoustic modes. (3) The phosphorene nanoribbons show the ultrahigh AR when the dimension ratio l/w is large, provided that we do not consider edge reconstruction.

In general, one may expect to choose a transport direction with higher thermal conductivity in electronic nanodevices whereas a direction with lower thermal conductivity in thermoelectric materials. These findings show the orientation controlled thermotability of phosphorene, as well as suggest a way to find out the optimized transport directions in phosphorene depending on its usage.

Acknowledgments

The work was supported in part by National Taiwan University "Aim for the Top University Plan" under Contract number 103R4000, and National Science Council Taiwan under Contract number NSC 102-2221-E-002-169-MY3. We are grateful to the National Center for High-performance Computing for computer time and facilities. We would like to acknowledge the suggestion by an anonymous referee to use the cosine function to represent the thermal conductivity. Part of this work was completed while the senior author (Chien-Cheng Chang) was visiting Guangxi University, Nanning, China.

References

- 1 A. K. Geim and I. V. Grigorieva, *Nature*, 2013, **499**, 419.
- 2 L. Li, Y. Yu, G. J. Ye, Q. Ge, X. Ou, H. Wu, D. Feng, X. H. Chen and Y. Zhang, *Nat. Nanotechnol.*, 2014, **9**, 372.
- 3 H. Liu, A. T. Neal, Z. Zhu, Z. Luo, X. Xu, D. Tománek and P. D. Ye, *ACS Nano*, 2014, **8**, 4033.
- 4 A. Ramasubramaniam and A. R. Muniz, *Phys. Rev. B*, 2014, **90**, 085424.
- 5 R. Fei and L. Yang, *Nano Lett.*, 2014, **14**, 2884.
- 6 X. Han, H. M. Stewart, S. A. Shevlin, C. R. A. Catlow and Z. X. Guo, *Nano Lett.*, 2014, **14**, 4607.
- 7 Q. Wei and X. Peng, *Appl. Phys. Lett.*, 2014, **104**, 251915.
- 8 J. Jiang and H. S. Park, *Nat. Commun.*, 2014, **5**, 4727.
- 9 H. M. Stewart, S. A. Shevlin, C. R. A. Catlow and Z. X. Guo, *Nano Lett.*, 2015, **15**, 2006.
- 10 Y. Cai, Q. Ke, G. Zhang, Y. P. Feng, V. B. Shenoy and Y. W. Zhang, *Adv. Funct. Mater.*, 2015, **25**, 2230.
- 11 J. B. Oostinga, H. B. Heersche, X. Liu, A. F. Morpurgo and L. M. K. Vandersypen, *Nat. Mater.*, 2007, **7**, 151.
- 12 D. Wei, Y. Liu, Y. Wang, H. Zhang, L. Huang and G. Yu, *Nano Lett.*, 2009, **9**, 1752.
- 13 Y. Zhang, T. Tang, C. Girit, Z. Hao, M. C. Martin, A. Zettl, M. F. Crommie, Y. R. Shen and F. Wang, *Nature*, 2009, **459**, 820.
- 14 S. Das, W. Zhang, M. Demarteau, A. Hoffmann, M. Dubey and A. Roelofs, *Nano Lett.*, 2014, **14**, 5733.
- 15 M. Buscema, D. J. Groenendijk, S. I. Blanter, G. A. Steele, H. S. J. van der Zant and A. Castellanos-Gomez, *Nano Lett.*, 2014, **14**, 3347.
- 16 W. Li, Y. Yang, G. Zhang and Y. W. Zhang, *Nano Lett.*, 2015, **15**, 1691.
- 17 A. A. Balandin, *Nat. Mater.*, 2011, **10**, 569.
- 18 J. Zhang, H. J. Liu, L. Cheng, J. Wei, J. H. Liang, D. D. Fan, J. Shi, X. F. Tang and Q. J. Zhang, *Sci. Rep.*, 2014, **4**, 6452.
- 19 B. L. Liao, J. W. Zhou, B. Qiu, M. S. Dresselhaus and G. Chen, Ab initio study of electron-phonon interaction in phosphorene, 2015, arXiv:1410.4242v4.
- 20 R. Fei, A. Faghaninia, R. Soklaski, J. Yan, C. Lo and L. Yang, *Nano Lett.*, 2014, **14**, 6393.
- 21 G. Qin, Q. Yan, Z. Qin, S. Yue, M. Hu and Gang Su, *Phys. Chem. Chem. Phys.*, 2015, **17**, 4854.
- 22 Z. Ong, Y. Cai, G. Zhang and Y. W. Zhang, *J. Phys. Chem. C*, 2014, **118**, 25272.
- 23 L. Zhu, G. Zhang and B. Li, *Phys. Rev. B*, 2014, **90**, 214302.
- 24 M. Born and K. Huang, *Dynamical theory of crystal lattices*, Oxford University Press, 1954.
- 25 J. Jiang, *Nanotechnol.*, 2015, **26**, 055701.
- 26 B. D. Kong, S. Paul, M. B. Nardelli and K. W. Kim, *Phys. Rev. B*, 2009, **80**, 033406.
- 27 L. Lindsay, D. A. Broido and N. Mingo, *Phys. Rev. B*, 2010, **82**, 161402(R).
- 28 T. H. Liu, Y. C. Chen, C. W. Pao and C. C. Chang, *Appl. Phys. Lett.*, 2014, **104**, 201909.
- 29 A. Jain and A. J. H. McGaughey, *Sci. Rep.*, 2015, **5**, 8501.
- 30 G. Chen, *Nanoscale energy transport and conversion: A parallel treatment of electrons, molecules, phonons, and photons*, Oxford University Press, 2005.
- 31 J. M. Ziman, *Electrons and phonons: The theory of transport phenomena in solids*, Oxford University Press, 1960.
- 32 C. J. Glassbrenner and G. A. Slack, *Phys. Rev.*, 1964, **134**, 1059.
- 33 D. T. Morelli, J. P. Heremans and G. A. Slack, *Phys. Rev. B*, 2002, **66**, 195304.
- 34 P. Giannozzi, S. Baroni, N. Bonini, M. Calandra, R. Car, C. Cavazzoni, D. Ceresoli, G. L. Chiarotti, M. Cococcioni, I. Dabo, A. Dal Corso, S. de Gironcoli, S. Fabris, G. Fratesi, R. Gebauer, U. Gerstmann, C. Gougoussis, A. Kokalj, M.

- Lazzeri, L. Martin-Samos, N. Marzari, F. Mauri, R. Mazzarello, S. Paolini, A. Pasquarello, L. Paulatto, C. Sbraccia, S. Scandolo, G. Sciauzero, A. P. Seitsonen, A. Smogunov, P. Umari and R. M. Wentzcovitch, *J. Phys.: Condens. Matter.*, 2009, **21**, 395502.
- 35 Z. Aksamija and I. Knezevic, *Appl. Phys. Lett.*, 2011, **98**, 141919.
- 36 Y. C. Chen, S. C. Lee, T. H. Liu and C. C. Chang, *Int. J. Therm. Sci.*, 2015, **94**, 72.
- 37 Y. Kôzuki, Y. Hanayama, M. Kimura, T. Nishitake and S. Endo, *J. Phys. Soc. Jpn.*, 1991, **60**, 1612.
- 38 T. H. Liu, S. C. Lee, C. W. Pao and C. C. Chang, *Carbon*, 2014, **73**, 432.
- 39 S. Ghosh, I. Calizo, D. Teweldebrhan, E. P. Pokatilov, D. L. Nika and A. A. Balandin, *Appl. Phys. Lett.*, 2008, **92**, 151911.
- 40 Y. Cai, J. Lan, G. Zhang and Y.W. Zhang, *Phys. Rev. B*, 2014, **89**, 035438.
- 41 K. Kaasbjerg, K. S. Thygesen and K. W. Jacobsen, *Phys. Rev. B*, 2012, **85**, 115317.
- 42 X. Jia, M. Hofmann, V. Meunier, B. G. Sumpter, J. Campos-Delgado, J. M. Romo-Herrera, H. Son, Y. P. Hsieh, A. Reina, J. Kong, M. Terrones and M. S. Dresselhaus, *Science*, 2009, **323**, 1701.
- 43 J. W. Jiang, H. S. Park and T. Rabczuk, *Appl. Phys. Lett.*, 2013, **114**, 064307.